I&EC research
Industrial & Engineering Chemistry Research

pubs.acs.org/IECR
Article

Understanding the Effect of Asphaltenes and Wax Inhibitors on Wax Crystallization by Improved NMR Techniques

George Claudiu Savulescu,* Sébastien Simon, Geir Sørland, and Gisle Øye

Cite This: https://doi.org/10.1021/acs.iecr.3c02218
Read Online

ABSTRACT: Wax crystallization represents one of the main factors impacting flow assurance during oil production. Pour point depressants (PPDs) and asphaltenes present in crude oil have been linked to modifications in wax crystallization behavior by cocrystallization and formation of complexes with wax. Wax precipitation has recently been assessed by low-field nuclear magnetic resonance (NMR) techniques. However, improvements remain to be made regarding the mechanism of the interactions between wax and the components that can alter the precipitated crystal network. In this article, wax−asphaltene and wax−PPD interactions were quantified by combining, for the first time, different low- and high-field NMR methods. First, the variation in the concentration of asphaltenes and PPD in solution with temperature was determined by a high-field NMR approach in model systems in the presence and in the absence of wax. Cocrystallization was demonstrated by observing a reduced content of asphaltenes and PPDs when wax was present. Second, the ratio between asphaltene monomers and nanoaggregates was quantified by low-field NMR relaxation time methods. Above a threshold asphaltene concentration, all asphaltenes were present as nanoaggregates. The same threshold concentration was associated with faster wax crystallization and an increase in the number of low-mobility dissolved wax molecules, interacting with the wax crystal network. Last, the impact of wax−PPD and wax−asphaltene crystallization patterns on the diffusion of the solvent through the wax network was quantified by using low-field NMR diffusion methods, followed by tortuosity calculations. Diffusion of solvent through the crystal network increased at higher asphaltene concentration and increased even further in the presence of PPD, indicating that these components lead to more open network structures. These new methods and breakthroughs about the wax precipitation mechanism may be extended to future studies of real crude oil systems.

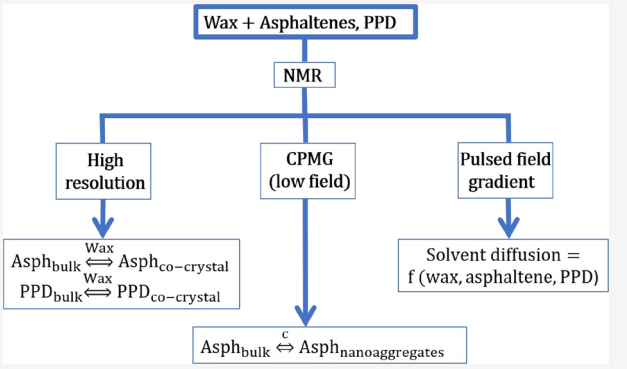

1. INTRODUCTION

Paraffin waxes are *n*-, iso-, or cycloalkanes with carbon chains between C_{18} and C_{100} or sometimes higher.[1] They are present in crude oils in varying concentrations, usually dependent on the oil field. There are 2 main types of waxes: macrocrystalline and microcrystalline. Macrocrystalline waxes have more linear structures and usually between 18 and 40 carbon atoms.[2] On the other hand, microcrystalline waxes contain iso-alkanes and cycloalkanes and usually have more than 40 carbon atoms.[2] Each waxy crude oil has a wax appearance temperature (WAT), at which wax starts to precipitate upon cooling. Subsequent gelation and deposition have a negative impact on flow assurance during crude oil production and transport. Several known effects are reduction of the crude oil flow in the pipeline, pressure abnormalities, pipeline restart issues, increased fluid viscosity, changes in the composition of the reservoir fluid, and in the worst case, a complete blockage of the flow.[3]

A conventional method to delay wax crystallization and to decrease the pour point below the industrial operating temperatures is the use of wax inhibitors, such as pour point depressants (PPDs).[4] PPDs are designed to show high affinity for the nonpolar moieties of wax, which often leads to cocrystallization or formation of complexes. These complexes undergo a crystallization mechanism different from that of pure wax crystals. The consequences are often higher solubility and altered crystal properties, such as lower aspect ratio and surface area.[5,6]

The presence of asphaltenes, polar components of crude oil, has also been demonstrated to affect wax precipitation. Asphaltenes are high molecular compounds in crude oil, insoluble in low molecular weight *n*-alkanes, such as hexane, but soluble in aromatic solvents, such as toluene.[7] At low concentrations, asphaltenes dissolve as monomers in toluene

Received: July 13, 2023
Revised: October 4, 2023
Accepted: October 6, 2023

or other aromatic solvents. However, as the concentration increases, asphaltenes start forming nanoaggregates (2−5 nm) at a concentration point often referred to as critical asphaltene concentration in the wax network (C.A.C.) or critical nanoaggregate concentration (C.N.A.C.).[8,9] As concentration increases further, the amount of asphaltene nanoaggregates will grow and secondary aggregation will begin through the formation of nanoclusters (>5 nm). These nanoaggregates and nanoclusters have often been referred to as nucleation sites for wax, generating more finely dispersed, smaller wax crystals inside the wax−asphaltene crystal network. While aggregated asphaltenes act as nucleation sites, the nonpolar groups of monomer asphaltenes are expected to act as connectors between the wax crystals, speeding the gelation process and increasing the gel strain but weakening the wax crystal network.[10−12] Although the modified crystals allow for better crude oil flow, they might increase WAT and the wax precipitation rate.[13−16,10,17] As expected from the opposing effects of asphaltenes, results of multiple studies generate contradicting conclusions about the role of asphaltenes during wax precipitation.[11] Some articles showed that asphaltenes inhibit wax precipitation in certain concentration regions but promote wax precipitation in other concentration regions, specific to each type of crude oil or wax−asphaltene model system.[9,18] The pattern of the concentration ranges for crystallization inhibition or promotion is in most cases irregular, probably because of the polydisperse character of asphaltenes and variable chemical composition of asphaltenes in each individual crude oil.[11,19] The exact mechanism behind the impact of asphaltenes on wax precipitation is not clear. That is the reason why this study aims to cover gaps in the literature by introducing a direct method to demonstrate cocrystallization of wax and asphaltenes. A second scope is to quantitatively investigate the effect of asphaltene nanoaggregation on wax precipitation.

Wax nucleation is affected not only by asphaltenes and PPDs but also by the addition of wax with different chemical compositions. Microcrystalline waxes are known to form gels with lower yield strength that precipitate at a lower rate than macrocrystalline wax.[2,20] Therefore, crystallization of macrocrystalline wax (linear alkane structure) has been investigated with and without the presence of microcrystalline wax (branched alkane structure).[21] When present, the microcrystalline waxes weakened the macrocrystalline wax crystal networks through spatial hindrances that prevent interlocking. This phenomenon leads to the formation of smaller and more finely dispersed macrocrystalline wax crystals, which make the system behave like a microcrystalline gel, despite the dominant macrocrystalline wax composition.[21]

The effect of wax inhibitors on wax crystallization was initially researched using multiple analytical methods such as differential scanning calorimetry (DSC), cross-polarized microscopy (CPM), and isothermal titration calorimetry (ITC). The analysis of wax precipitation by low-field NMR was introduced by Pedersen et al., who calculated wax content in crude oil, from relaxation time data.[22] In recent years, wax crystallization has been characterized by an adapted Carr−Purcell−Meiboom−Gill (CPMG) sequence,[23,24] which focuses on the effect of asphaltene and PPD in model wax-based systems. The temperature dependence of the percentage of solid in model wax and wax−PPD systems was assessed by Zhao et al. with NMR CPMG.[25] Ruwoldt et al. extended the range of PPDs used in the wax-based systems and considered the influence of asphaltenes for the first time.[26] An advantage of NMR compared to DSC was the use of fewer thermodynamic assumptions to determine the wax content. In this study, the authors identified for the first time a transition of a low-mobility dissolved wax. The newly formed wax−asphaltene particles interact with dissolved wax molecules, trapping them and decreasing their mobility. Starting from this finding, Savulescu et al.[19] proposed a method to characterize both the evolution of wax precipitation rate and the evolution of dissolved wax mobility in wax−asphaltene and wax−PPD model systems. Their study found that a threshold asphaltene concentration generated an increase in the amounts of both precipitated wax and dissolved wax trapped inside the crystal network. Formation of asphaltene nanoaggregates acting as nucleation sites for wax and interactions between the altered wax−asphaltene crystal network and dissolved wax were indicated as potential causes for these observations. Regarding the PPD, its presence was observed through a low mobility peak, which disappeared once wax precipitation stars, due to complex formation and subsequent cocrystallization between wax and PPD.

The previous studies referred to cocrystallization and complex formation without providing quantitative proof. This article aims to remove this ambiguity and comes as a continuation of the previous work.[19] The first focus is the demonstration of wax−asphaltene and wax−PPD cocrystallization with high-resolution NMR. Second, a quantitative link between asphaltene nanoaggregation state and wax precipitation was studied using an adapted CPMG sequence. Last, the focus shifted toward the diffusion of the solvent to understand the effect of PPD and asphaltenes on flowability during wax crystallization. The restricted and unrestricted diffusion coefficients were calculated using diffusion-focused low-field NMR. The sum of these three sections improved the knowledge of the wax crystallization mechanism in the presence of asphaltenes or PPD.

2. EXPERIMENTAL SECTION

2.1. Materials. The solvents used in this study were deuterated toluene (anhydrous, 99.6% deuterated), toluene (anhydrous, 99.8%) from Sigma-Aldrich, Norway, and extra pure deuterated toluene (99.94%) from ChemSupport AS, Norway. Macrocrystalline and microcrystalline waxes were provided by Sasolwax from Sasol, Germany (wax 5405 and 3971, respectively). The composition and properties of these wax samples were presented previously.[26] Asphaltenes were precipitated from a crude oil (API 19°) originating from the Norwegian shelf of the North Sea, using *n*-hexane (HPLC grade, ≥97%), and the same procedure as reported before.[19] Properties of the asphaltenes precipitated from this crude oil were also published previously.[27,28] The pour point depressant was based on polycarboxylate (proprietary) from BASF, Germany, and was presented as PPD A by Ruwoldt et al.[26] and as PPD by Savulescu et al.[19] The PPD was solvent-purified using the procedure detailed previously.[26] All concentrations presented in this study are in weight percentages (wt %).

2.2. Experimental Techniques. *2.2.1. Sample Preparation.* To prepare the samples for high-resolution NMR analysis, PPDs and asphaltenes were first dissolved in deuterated toluene (99.6%), obtaining stock solutions with concentrations of 1.05 and 2.1 wt %, respectively. These were shaken overnight at 200 rpm to ensure complete dissolution. Then, a range of wax−PPD and wax−asphaltene solutions

https://doi.org/10.1021/acs.iecr.3c02218
Ind. Eng. Chem. Res. XXXX, XXX, XXX−XXX

were prepared by dilution of the initial solutions, and the desired macrocrystalline wax content was added. A range of wax-only solutions was also prepared by dissolution of wax in deuterated toluene. All wax-containing systems were heated at 60 °C for 1 h and shaken thoroughly. Last, the NMR tubes were filled to a line of 40 mm. The solubility of asphaltenes at a high concentration (2%) in the wax−asphaltene system was further confirmed with an optical microscope. For wax−PPD mixtures, macrocrystalline wax was chosen, while for wax−asphaltene mixtures, microcrystalline wax was used. Each type of wax was scanned individually with high-resolution NMR.

For NMR CPMG, a stock solution of 2% asphaltene was prepared in extra pure deuterated toluene (99.94%) to ensure an extremely low content of residual hydrogenated solvent (max 0.06%) in asphaltene-only solutions. Dissolved asphaltene monomers and hydrogenated toluene have NMR signals in the same relaxation time region (high mobility). Therefore, the low concentrations of asphaltenes used in this study determined the necessity of reducing the residual hydrogenated solvent to the highest achievable extent. A range of asphaltene solutions with concentrations ranging from 0.2 to 2% was prepared by diluting the stock solution. All of the solutions were shaken overnight at 200 rpm to optimally dissolve the asphaltenes. Then, 3 g of each was transferred into NMR tubes for scanning.

For the tortuosity measurements, there were 3 differences in preparation of the solutions compared to the sample preparation for high-resolution NMR. The first is that the solvent was hydrogenated toluene, instead of deuterated toluene. The second is that for tortuosity measurements, the quantity of solution in the measurement tube was 3 g. The last difference is that the type of wax for all systems was a macrocrystalline wax.

Two independent parallels were performed with NMR for each system to ensure reproducibility. The overall error was calculated from the variation between the 2 parallels, and it is displayed in the corresponding figures.

2.2.2. Nuclear Magnetic Resonance: High-Field Analysis. For the high-field NMR study, a Bruker 600 MHz Avance III HD equipped with a 5 mm cryogenic CP-TCI z-gradient probe was used. The chemical spectra were acquired isothermally at 30, 10, and 0 °C, with 15 min allowed for temperature stabilization before each scan. The selected temperatures were determined by the wax appearance temperature, which is between 15 and 25 °C for the selected systems.[19,26] The residual toluene signals were expected to increase with lower temperature but only as a consequence of signal fluctuation induced by the temperature change.[23] Therefore, they were considered as a reference to normalize the other signals, which were used for the quantitative analysis of each species.

The reason for the choice of microcrystalline wax for wax−asphaltene mixtures (Section 2.2.1) was the inability to obtain accurate high-resolution NMR data with asphaltenes and macrocrystalline wax at low temperature. Wax−asphaltene precipitation generated a sharp drop in diffusion values and a high level of heterogeneity in the sample, which altered the consistency of the values for signal intensity: the reference residual toluene had a drop in signal, although the toluene molecules remained in the same phase (Figure S1a,b in the Supporting Information). This is because of strong radiation damping effects that distort the liquid signal when inhomogeneity is present. The high-field NMR is more sensitive than the low-field NMR and cannot record low mobility or a low diffusion signal in inhomogeneous systems. To decrease the heterogeneity of the wax−asphaltene system at low temperature, the microcrystalline wax with lower viscosity and a lower precipitation rate[20] was used.

2.2.3. Nuclear Magnetic Resonance: CPMG Analysis. Low-field NMR studies were performed using a 21 MHz NMR spectrometer supplied by Anvendt Teknologi AS, Norway. A CPMG procedure was used to acquire T_2 distributions for asphaltene-only solutions in extra pure deuterated toluene,[24] following the procedure presented previously.[19] The recycle delay was in this case 5 s, while the inter-echo spacing was selected to adapt for the low signal expected from 0.2 to 2% asphaltene-only solutions. A first region was selected at τ_1 of 200 μs and with 1000 echoes to account for the short T_2 region for low-mobility molecules (asphaltene nanoaggregates) and a second region was selected at τ_2 of 600 μs and with 3000 echoes for the long T_2 region for high-mobility molecules (asphaltene monomers). The number of scans was 128, except for the 0.2% asphaltene system, where 512 scans were needed to compensate for the very low signal. After acquiring raw CPMG data, a map of the proton intensity at each T_2 was generated from the multiexponentially decaying curve using the Anahess/one-dimensional Inverse Laplace Transform approach.[29] The proton intensity at each T_2 is a quantitative measure of the liquid signal, which allows for the quantification of high- and low-mobility asphaltene regions. A boundary was set between the two mobility regions for asphaltene at a T_2 of 0.5 s. Values above this threshold are specific to pure solvents at 30°C (hexane and toluene), and therefore, they most likely correspond to dissolved asphaltene monomers with high mobility in the analyzed systems or to residual toluene. However, the amount of residual toluene is very low, since 99.94% pure deuterated solvent was used. Moreover, a decrease of about 70% in the high peak intensity occurred when the asphaltene concentration was increased (Section 3.2), demonstrating that the contribution of the residual hydrogenated toluene in the peak is negligible. Figure S2 in the Supporting Information confirmed the peaks for hexane and toluene at high T_2 (10^0 to 10^1 s). The same values could be observed for high T2 peaks in Section 3.2 in this study for asphaltene-only systems. Previous studies have confirmed that model asphaltene monomers have a diameter of around 15−20 Å,[30] which is about 2−3 times higher than for toluene (5−6 Å).[31] T_2 values for toluene monomers should be slightly higher than for asphaltene monomers, but the measurement showed that they are in the same range (1−10 s). When it came to T_2 peaks at values below the threshold at T_2 = 0.5 s, they were associated with larger asphaltene nanoaggregates and nanoclusters, whose mobility and T_2 value decreased. However, low-field NMR was not able to distinguish between nanoaggregates and nanoclusters, as the relation between the exact molecular size and the T_2 could not be quantified directly to an extent that would allow separation between sizes of 2−5 nm and >5 nm.

The asphaltene experiments were performed isothermally at 30 °C after allowing 15 min for the temperature to stabilize. The temperature inside the NMR was controlled by using an integrated temperature controller connected to the NMR system.

2.2.4. Nuclear Magnetic Resonance: Tortuosity Determination. A pulsed field gradient-stimulated echo sequence with bipolar gradients[32] was used to acquire the diffusion coefficient at increasing observation times (Δ). Also, a pulsed field

https://doi.org/10.1021/acs.iecr.3c02218
Ind. Eng. Chem. Res. XXXX, XXX, XXX−XXX

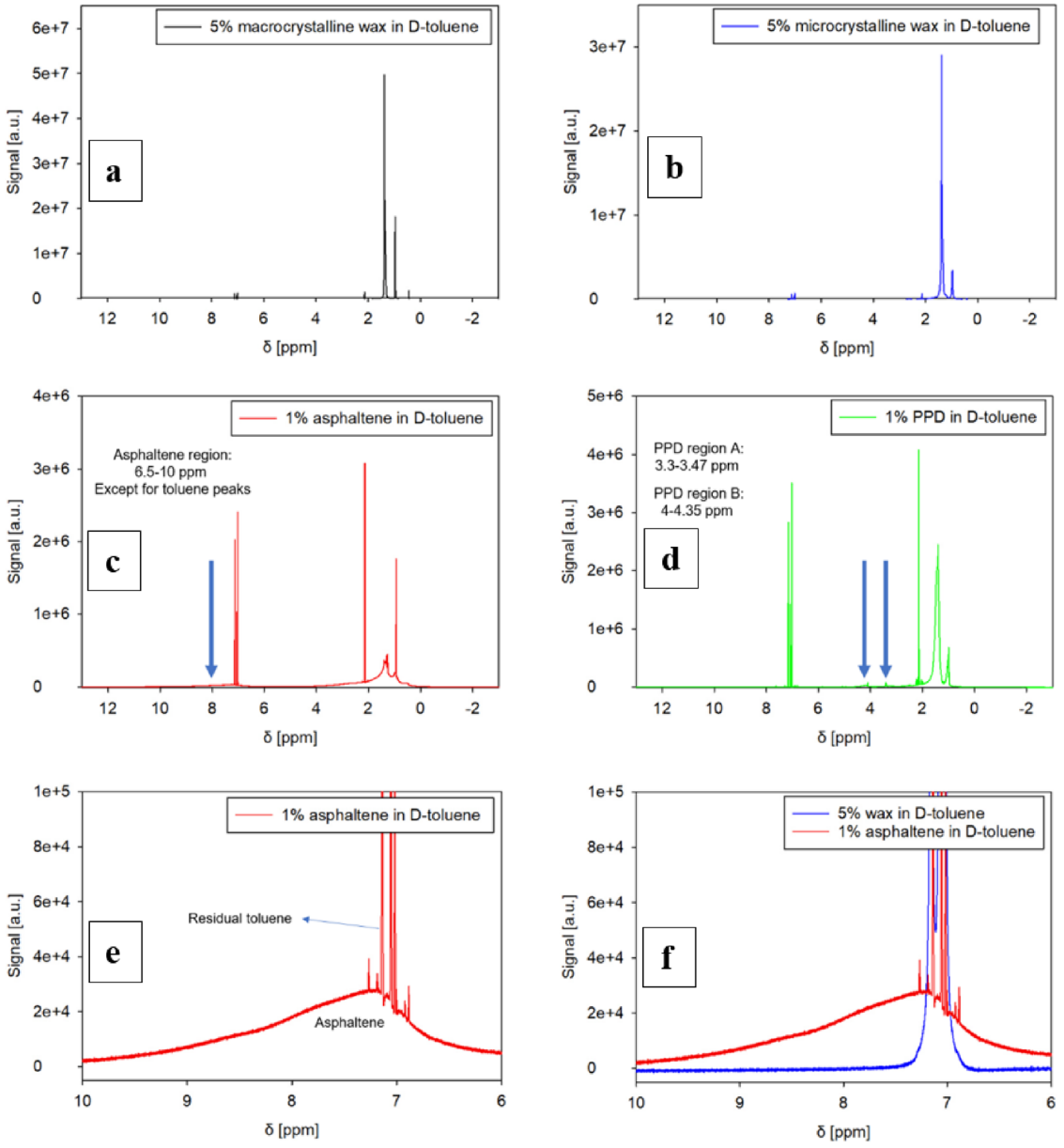

Figure 1. (a–d) ^{1}H NMR spectrum for (a) 5% macrocrystalline wax in deuterated toluene, (b) 5% microcrystalline wax in D-toluene, (c) 1% asphaltene in deuterated toluene, and (d) 1% PPD in deuterated toluene; (e, f) slices from 10 to 6 ppm in the ^{1}H NMR spectrum for (e) 1% asphaltene in deuterated toluene and (f) 5% microcrystalline wax in deuterated toluene, with a comparison to 1% asphaltene in deuterated toluene. Markings for inhibitor-specific peaks indicate the corresponding regions in panels (c) and (d).

gradient spin echo sequence with bipolar gradients[33] was used to measure the diffusion coefficient at the shortest observation time possible. The sequence for the pulses is summarized graphically in Figure S3 in the Supporting Information. The samples were scanned isothermally at 30, 10, and 0 °C, with 15 min for temperature stabilization before each acquisition. The diffusion was acquired over a range of values, starting from 2.7 ms (the dead time of the instrument) to 1000 ms. The tortuosity factor is usually calculated as the ratio between free diffusion (at zero observation time) and restricted diffusion (at 1000 ms).[34,35] In this study, the tortuosity was calculated using the point at 2.7 ms for the free diffusion. Extrapolation to 0 ms would have been inaccurate because of the low number of data points at very short times (<30 ms). The restricted diffusion coefficient is acquired at very long times, at which the displacement of the diffusing solvent molecules through the constricting space is much larger than the length scale of the constricting space.[35,36] Thus, the measured diffusion coefficient approached an asymptotic value, independent of the measurement time but dependent on the constricting space, which in this case was the resulting wax or wax–inhibitor crystal networks and the corresponding intermediate gels.

3. RESULTS AND DISCUSSION

3.1. Cocrystallization of Wax and Asphaltenes and PPD. *3.1.1. Choice of Resonance Domain.* High-resolution NMR was used to determine the cocrystallization of wax with asphaltenes and PPDs quantitatively. This was performed by determining the variations of the intensity of the NMR peaks specific to the asphaltenes and wax at temperatures above and below the wax appearance temperature. The first step was to compare the spectra of the wax with the spectra of the

https://doi.org/10.1021/acs.iecr.3c02218
Ind. Eng. Chem. Res. XXXX, XXX, XXX−XXX

asphaltenes and PPD. The purpose was to determine asphaltene-specific and PPD-specific regions in the spectra, which afterward could be used to determine their intensity in the liquid state in wax−asphaltene and wax−PPD systems. High-resolution NMR signals focused on the high-mobility liquid region, so any decrease from the wax (macrocrystalline and microcrystalline), asphaltene, and PPD peaks could be linked to the phase change toward very-low-mobility liquid or solid states. The detection limit remained a limitation of the method because the exact diffusion value at which the signal is lost was unknown.

Figures 1a−d illustrates that a signal specific to chemical shifts for aliphatic hydrogen atoms developed for all four systems at 0.8−3 ppm. The distribution of the signal inside the 0.8−3 ppm interval varies for wax, asphaltenes, and PPD due to different chemical compositions. For macrocrystalline wax, this corresponds to $-CH_3$ and $-CH_2$ groups, while for microcrystalline wax, this most likely corresponds to $-CH_3$, $-CH_2$, and −CH groups.[21,26] The small difference between relevant chemical shifts and the very high percentage of protons from wax in wax−inhibitor systems made the compositional determination inaccurate. Therefore, the focus for inhibitor-specific regions was placed on chemical shifts above 3 ppm. For PPD, two weaker peaks were observed at 3.3−3.47 and 4−4.35 ppm, referred to as PPD region A and PPD region B, respectively. These regions most likely correspond to alcohol or ester groups present in the structure of the PPD. The difference between the 2 regions was associated with the difference between the types of carbon with which the oxygen atom bonds with. For example, $-CH_2-O-$ groups were expected to generate a signal at a slightly higher chemical shift than CH_3-O- groups. Figure S4 presents a comparison between the PPD spectrum and the macrocrystalline wax spectrum inside the 3−5 ppm region and confirms that only the PPD generated a positive signal inside this region. For asphaltenes, a signal was found from 6.5 to 10 ppm (Figure 1 e,f). This region overlapped with aromatic components of residual toluene from 7.5 to 6.75 ppm. These toluene peaks were deducted from the total signal of the region to calculate the asphaltene-specific signal. The asphaltene signal in this region was generated by aromatic components in the asphaltene structure. One can notice in Figure 1 e,f that the spectrum for 5% wax only recorded the aromatic part of the residual toluene in the 6.75−7.5 ppm interval.

3.1.2. Evolution of Inhibitor Content during Wax Crystallization. After the identification of the inhibitor-specific resonance domains, the second step of the analysis of high-resolution NMR results was the quantification of inhibitor-specific signals with temperature in the wax−inhibitor model systems.

3.1.2.1. Wax−PPD Cocrystallization. The evolution of the two PPD-specific regions (A and B) with the temperature is quantified in Figure 2. The decrease in the PPD signal with decreasing temperature demonstrated that the parts of PPD corresponding to region A and region B underwent either precipitation or a strong decrease in diffusion from 30 to 0 °C and, in particular, between 10 and 0 °C. This was not the case for all the chemical species of the PPD, as one can notice in Figure S5 in the Supporting Information. The region between 0.8 and 3 ppm (aliphatic) only recorded an insignificant decrease from 30 to 0 °C. This showed that regions A and B behaved different than the rest of the PPD. However, A and B represented about 1.5% of the total proton signal and

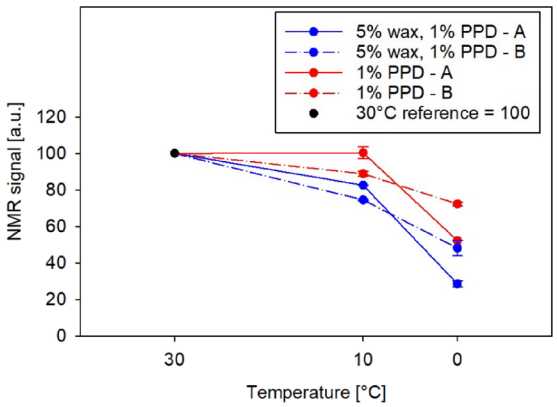

Figure 2. Variation of signal with temperature for PPD-specific peaks A and B in 5% macrocrystalline wax, 1% PPD in deuterated toluene, and 1% PPD in deuterated toluene. The value at 30 °C is fixed at 100 for all systems, while the values at 10 and 0 °C are normalized accordingly.

corresponded to polar groups such as esters, which are connected to a larger chemical structure with a polar and nonpolar part, the latter of which has a high likelihood to interact with wax.[37]

In the wax−PPD system, the relative intensity of region A at 0 °C was 28% lower than that in the PPD-only system. Region B had a relative intensity at 0 °C that was 42% lower in the wax−PPD system than that in the PPD-only system. The decrease in liquid PPD in the presence of wax indicated cocrystallization and could be agreed with studies in the literature, which demonstrated complex formation between wax and PPD in the dissolved state, followed by complex crystallization. PPDs are also known to modify wax crystals by being incorporated in the wax crystal network and then imposing steric hindrance on further wax crystal network evolution.[2,5]

It is worth noting that in a previous study, it was found by NMR CPMG that the addition of 1% PPD decreased the average wax precipitation rate by about 30% at 0 °C.[19] Using high-resolution NMR, on the other hand, the average wax precipitation rate decreased by only 12−15% upon addition of PPD (Figure 3). The main reasons for the difference between the two methods are the assumptions behind the calculations

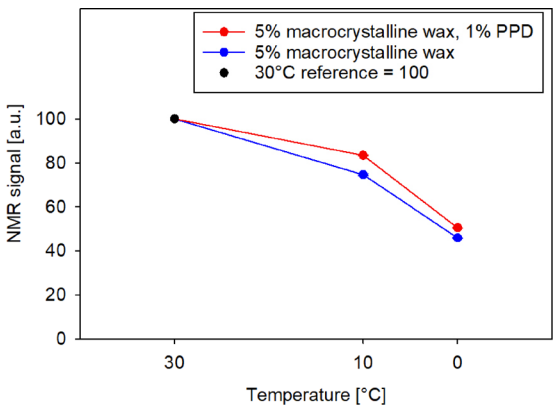

Figure 3. Variation of signal of aliphatic peak with temperature for 5% macrocrystalline wax and 5% macrocrystalline wax with 1% PPD, both in deuterated toluene. The value at 30 °C is fixed at 100 for all systems, while the values at 10 and 0 °C are normalized accordingly.

https://doi.org/10.1021/acs.iecr.3c02218
Ind. Eng. Chem. Res. XXXX, XXX, XXX−XXX

for each of the methods and the detection limit, which is higher for high-resolution NMR (higher radiation damping).

3.1.2.2. Wax–Asphaltene Cocrystallization. To check whether the asphaltene-specific aromatic region was representative for the whole asphaltene sample, its evolution with temperature was compared with the evolution of the aliphatic region (Figure S6 in the Supporting Information). A quasi-similar decrease was noticed from 30 to 0 °C, but there are some small differences at 10 °C, most likely due to the polydispersity of asphaltenes. The high proportion of aromatic signal in the total signal (6–7%) also consolidated the fact that the asphaltene-specific signal was representative for the entire range of asphaltene species for the purpose of this study.

The next step was the investigation of the asphaltene signal in the presence and absence of wax (Figure 4). One can notice

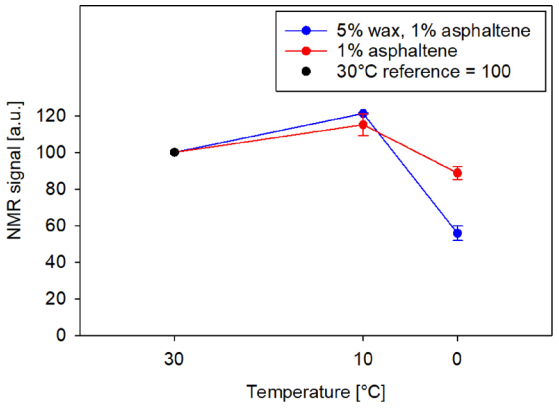

Figure 4. Variation of signal with temperature for asphaltene-specific peak in 5% microcrystalline wax, 1% asphaltene in deuterated toluene, and 1% asphaltene in deuterated toluene. The value at 30 °C is fixed at 100 for all systems, while the values at 10 and 0 °C are normalized accordingly.

a slight increase of signal from 30 to 10 °C, which corresponded to signal fluctuation induced by the difference in energy levels of atoms as a result of thermal change.[23] Consequently, one can conclude that no transition toward solid or aggregate phases occurred at 10 °C. However, when the temperature was decreased to 0 °C, the asphaltene-specific peak in the asphaltene-only system decreased by about 15%, while the one in the wax–asphaltene system decreased by about 45%. The former could be linked with asphaltene aggregation,[38] which caused a decrease in the diffusion of asphaltenes to very low values, outside of the measured liquid range. The latter demonstrated a marked decrease in the level of asphaltene diffusion when wax was present. This emphasized the interaction between asphaltenes and wax during wax gelation and crystallization and demonstrated cocrystallization. The additional decrease in asphaltene liquid signal could also be associated with a higher rate of nanoaggregate formation and even flocs, incorporated in the newly formed wax crystal networks. This supported the hypothesis that nonpolar parts of the dissolved monomers and nanoaggregate asphaltenes interact with the nonpolar wax molecules, forming wax–asphaltene networks that crystallize together.

The rate of wax–asphaltene precipitation was also quantified using the aliphatic region (Figure S7). This region consisted mainly of wax due to the weak proton signal coming from asphaltenes. A reduction of 4–6% in the wax precipitation rate was noticed at both 10 and at 0 °C. Asphaltenes were therefore inhibiting microcrystalline wax at these temperatures. Moreover, one can also notice in Figure S7 that wax precipitation was taking place at both 10 and 0 °C. However, asphaltene precipitation started between 10 and 0 °C, which implies that there was a delay between the wax appearance point and wax–asphaltene coprecipitation point. When analyzed with NMR CPMG, the same system generated a low-mobility wax region, corresponding to trapped dissolved molecules inside the newly formed crystal network, with a similar delay from the start of wax precipitation.[19] This demonstrated that during the gelation phase, the trapping of dissolved wax is accelerated by the formation of wax–asphaltene cocrystals.

In their study with NMR CPMG, Savulescu et al.[19] concluded that asphaltenes exceeding a threshold concentration, estimated to be 0.75%, enhanced the amount of low-mobility dissolved wax trapped inside the crystal networks and promoted wax precipitation. Formation of larger asphaltene nanoaggregates and nanoclusters was indicated as a potential cause of this effect. Findings in Figure 4 present a system with asphaltenes above the threshold concentration. Thus, the decrease in asphaltene liquid content observed with high-resolution NMR was most likely caused by the presence of larger asphaltene nanoaggregates or nanoclusters, which interfered with wax crystallization by acting as nucleation sites or by binding to wax through nonpolar moieties. This study aimed to quantify the asphaltene aggregation state at various asphaltene concentrations and link it to patterns in wax crystallization. Therefore, the second part of the results section

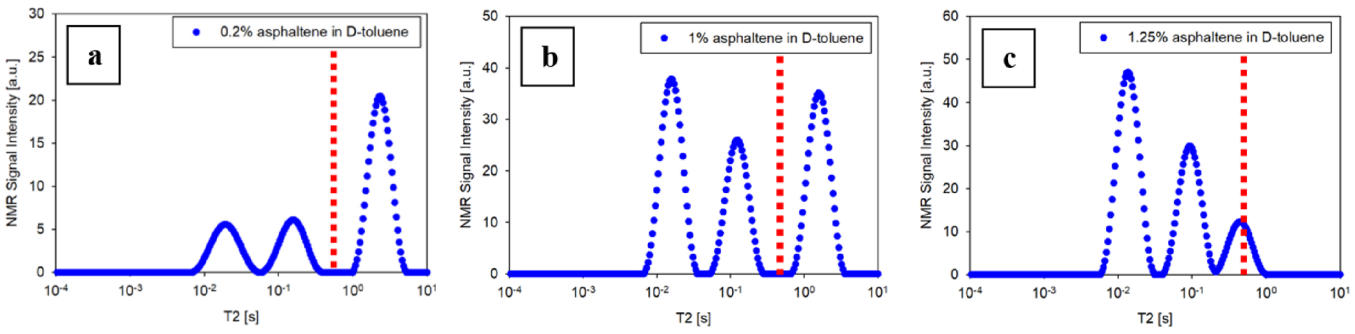

Figure 5. Relaxation time distribution in liquid domain for (a) 0.2% asphaltene in deuterated toluene, (b) 1% asphaltene in deuterated toluene, and (c) 1.25% asphaltene in deuterated toluene. The red line marks the border between high-mobility asphaltene monomers and low-mobility asphaltene nanoaggregates.

https://doi.org/10.1021/acs.iecr.3c02218
Ind. Eng. Chem. Res. XXXX, XXX, XXX–XXX

will focus on the determination of the monomer/aggregate ratio in asphaltene-only systems.

3.2. The Effect of Asphaltene Nanoaggregation State on Wax Precipitation. T_2 relaxation times measured by NMR CPMG were correlated with the mobility of hydrogen species. The higher the mobility, the higher the T_2. As the mobility is a function of the size of molecular species/aggregates, measuring the T_2 distribution of a sample allowed us to probe the size distribution of molecules or aggregates present in the sample. It is worth noting that the T_2 distributions were highly reproducible (Figures S8 and S9 in the Supporting Information).

Figure 5a presents the distribution of T_2 relaxation times for the system with the lowest concentration (0.2%) of asphaltenes. This minimum concentration was selected after taking into consideration the limitations of NMR resonance frequency detection. Figure 5a comprises of 3 signal peaks, a stronger one that formed in the asphaltene monomer region (T_2 > 0.5 s) and two weaker ones in the asphaltene nanoaggregate/nanocluster region. As the asphaltene concentration was increased to 1%, the distribution of the peaks changed and the signal in the nanoaggregate/nanocluster region had higher relative intensity compared to the monomer signal (Figure 5b). This pattern intensified when the concentration was increased to 1.25% asphaltenes, where little to no monomer peak signal was observed (Figure 5c). This indicated an almost complete shift in equilibrium toward >90% nanoaggregates/nanoclusters between 1 and 1.25% asphaltenes. The total intensity of the signal (Figure 6) also followed

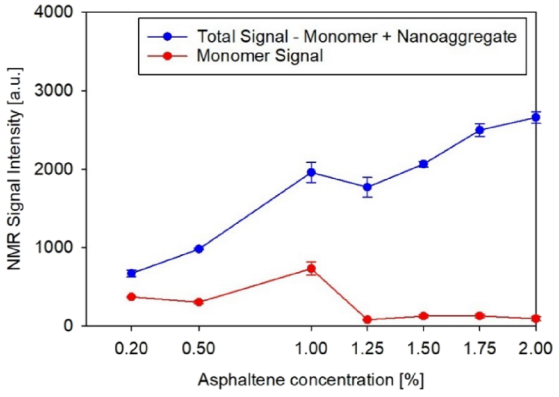

Figure 6. Total signal and monomer signal as a function of asphaltene concentration in asphaltene-only solutions in deuterated toluene.

a modified pattern from 1 to 1.25%. The signal varied linearly with asphaltene concentrations below 1% and above 1.25%. However, from 1 to 1.25%, the total signal was almost constant, indicating that part of the asphaltenes aggregated or clustered to such an extent that they underwent loss of mobility, which shifted the T_2 to a value below the measured range.

This observation was linked to previous findings,[19] where asphaltenes reaching a threshold concentration of 0.75% promoted wax precipitation and provided reduced mobility on dissolved wax molecules, which became trapped in the gaps of the wax−asphaltene cocrystal network or in the wax−asphaltene cocrystal pores. This process prevented further crystal growth.[19] The asphaltene nanoaggregation state was highlighted as the reason for the change in behavior. Thus, the demonstration of the complete shift from monomer to aggregates/clusters at 1.25% asphaltene confirmed the explanation in the previous article. However, a gap remains between the asphaltene concentration at which the shift was observed: 0.75% in wax−asphaltene systems and 1.25% in asphaltene-only systems. Two potential explanations arise for this gap. First, the previous experiments were performed dynamically from 45 to 0 °C. The change in wax precipitation behavior and the intensification of the amount of trapped dissolved wax were observed at temperatures lower than 15 °C when wax started precipitating. In the current study, the temperature was isothermally set at 30 °C. The asphaltenes were expected to form larger nanoaggregates/nanoclusters with lower mobility at lower temperature,[39] which would decrease the threshold concentration. The second explanation is that the factor triggering the changes in wax precipitation behavior was not the complete shift toward nanoaggregates/nanoclusters but the shift toward a threshold nanoaggregate/nanocluster content relative to the wax content. Figures 6 and 7 solidify this hypothesis. Although the monomer and

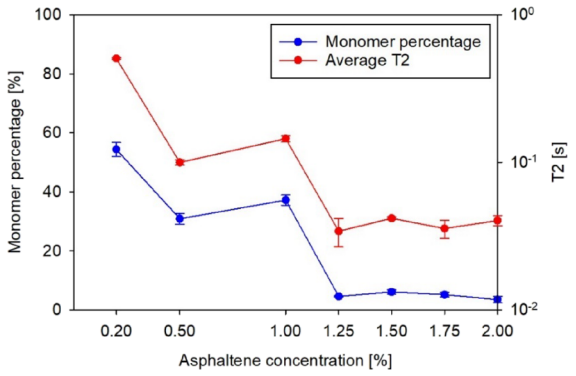

Figure 7. Monomer percentage and average T_2 (monomer + nanoaggregate/nanocluster) as a function of asphaltene concentration in asphaltene-only solutions in deuterated toluene.

nanoaggregate/nanocluster percentages were quasi-constant from 0.5 to 1% asphaltene, the amount of nanoaggregates/nanoclusters was approximately 2-fold in the system with 1% asphaltene. When the wax concentration was fixed, the ratio between nanoaggregate/nanoclusters and wax became twice as high at 1% asphaltene compared to 0.5% asphaltene. The asphaltene nanoaggregate/nanocluster to wax ratio was thus likely to dominate the wax precipitation behavior.

Another observation in Figure 6 is the shift in nanoaggregate/nanocluster percentage that occurred from 0.2 to 0.5%. At a low asphaltene concentration, the nanoaggregate/nanocluster content was very low. This was associated with a different behavior of wax−asphaltene systems with a very low asphaltene concentration. For example, previous studies concluded that low asphaltene content could lead to wax precipitation inhibition.[9,26] A lower content of nanoaggregates/nanoclusters could be associated with a lower likelihood for asphaltenes to act as wax nucleation sites, which explains why the precipitation was not accelerated. Simultaneously, asphaltenes were still present in the monomer state, which implied that they could act as wax binders and modify crystal networks, preventing normal crystal growth. The equilibrium between the latter and former effects is most likely a function of the total asphaltene concentration. Thus, at low asphaltene concentrations, the former effect dominated, making inhibition

https://doi.org/10.1021/acs.iecr.3c02218
Ind. Eng. Chem. Res. XXXX, XXX, XXX−XXX

more likely, while at high asphaltene concentrations, the latter effect dominated, making promotion more likely.

The results analyzed so far were consolidated through the quantification of the average T_2 (Figure 7), which has a quasilinear trend similar to the monomer percentage. This observation reaffirmed the choice of T_2 at 0.5 s as a border between the monomer and the nanoaggregate: the loss in monomer percentage accounts for the loss in mobility that occurs with increasing concentration.

The formation of asphaltene nanoaggregates and nanoclusters was demonstrated before with SAXS and SANS.[8,40−42] However, the quantification of the monomer:nanoaggregate ratio represents a novelty in asphaltene research.

3.3. The Effect of Asphaltenes and PPDs on the Diffusion of Solvent through the Wax Crystal Network.

The previous subsections focused on the evolution of the molecular mobility of the inhibitors in wax−inhibitor systems. The last subsection will focus on the diffusion of the solvent to understand how modifications in the wax crystal networks affect the mobility of dissolved molecules.

Figures 8 and 9 present the diffusion coefficient as a function of time for the liquid species, representing toluene and the

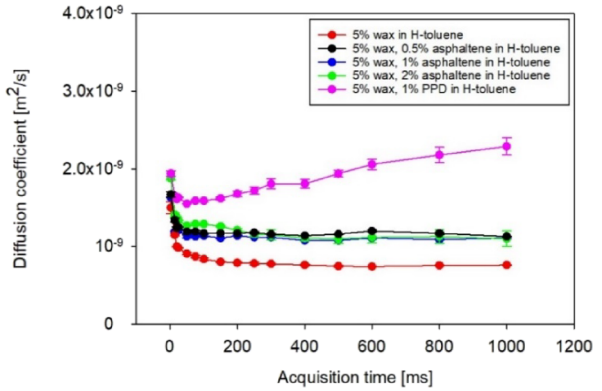

Figure 8. Diffusion coefficient profile at 10 °C as a function of acquisition times for wax, wax−asphaltene, and wax−PPD systems in toluene.

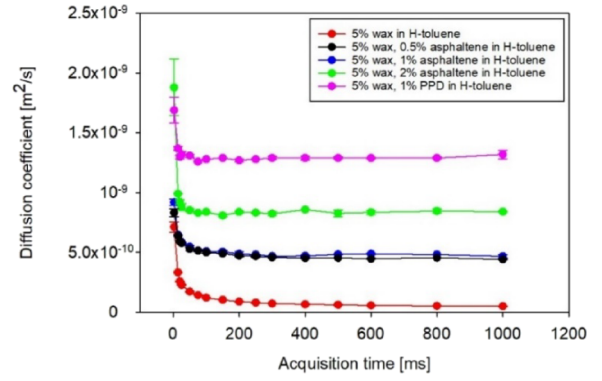

Figure 9. Diffusion coefficient profile at 0 °C as a function of acquisition times for wax, wax−asphaltene, and wax−PPD systems in toluene.

remaining dissolved species (<7%) at 10 and 0 °C (i.e., below the WAT), respectively. The calculated diffusion coefficients represented the remaining fluid during wax crystallization and were mostly influenced by the diffusion of toluene molecules (>93%). The precipitation of wax was expected to impact the free diffusion coefficient of the solvent molecules. One can observe in Figure 9 that at 0 °C, the diffusion coefficient decreased exponentially at short times and then remained constant at longer times. The coefficient at zero time corresponds to the unrestricted diffusion coefficient, while the coefficient at high time is the restricted diffusion coefficient, which results from the solvent being surrounded by the wax crystal network.

The values at the first measured point were closer to the self-diffusion values for toluene from the literature, but there were some deviations. For example, the literature value for self-diffusion of toluene at 0 °C was 1.5×10^{-9} m^2/s,[43] while the unrestricted diffusion values determined at 2.7 ms were in the range of 7×10^{-10} to 1.8×10^{-9} m^2/s for the wax-based systems (Figure 9). One reason for this discrepancy was the presence of dissolved wax or asphaltenes, which altered the liquid diffusion value from the toluene value. Another reason was the restriction imposed already during the dead time (2.7 ms). To demonstrate this, one can notice that the lower the unrestricted diffusion coefficient, the lower the restricted diffusion coefficient (Figure 9).

The restricted diffusion coefficient was 5−9 times higher when asphaltenes were present at 0 °C (Figure 9). The difference was lower at 10 °C (Figure 8): the restricted diffusion coefficient was higher by about 30% when asphaltenes were added and was not sensitive to the asphaltene concentration. At both temperatures, the increase in the restricted diffusion coefficient could be linked to the alteration of the wax crystal network generated by the asphaltenes.[11] The higher solvent diffusion indicated less restriction imposed by the altered wax−asphaltene crystal network on the solvent molecules. This was consistent with previous cross-polarized microscopy results that demonstrated smaller, more finely dispersed crystals when asphaltenes were present.[26] An increased asphaltene concentration (2%) could be associated with significantly less restriction on the solvent molecules but only at 0 °C when the precipitation reached a certain threshold (Figures 8 and 9). This confirmed that high asphaltene concentration induced more open crystal networks, which led to higher solvent flowability.

A different pattern can be observed for the wax−PPD system in both Figures 8 and 9. At 10 °C, it followed a similar decreasing exponential pattern at low acquisition times (Figure 8). However, there was a shift to a linear increase at high times. This demonstrates that in the wax−PPD system, the amount of solid was not high enough at 10 °C to form a network, and therefore, the system still behaved partially like a liquid. When the gel forms, only Brownian motion influences the diffusion coefficient at high times. On the other hand, for liquids, convection distorts the NMR signal, generating the linear increase observed for the wax−PPD system at high times. Consequently, one can conclude that the PPD inhibited gel formation, which was otherwise undergoing at the same temperature in the wax system without PPD. When the temperature was decreased to 0 °C (Figure 9), the linear increase was not present anymore, which demonstrated that the newly precipitated solid wax prevented convection. The restricted diffusion coefficient for wax−PPD was about 13 times higher than that for wax only. The reason was the formation of a highly altered wax crystal network, with smaller and more dispersed crystals, as described in the literature.[2,5]

Tortuosity values derived from the diffusion coefficients in Figures 8 and 9 are presented in Figures S10 and S11 in the

https://doi.org/10.1021/acs.iecr.3c02218
Ind. Eng. Chem. Res. XXXX, XXX, XXX−XXX

Scheme 1. Model Schematics for Crystal Networks and Liquid Phases for Wax and Wax−asphaltene Systems at 0 °C

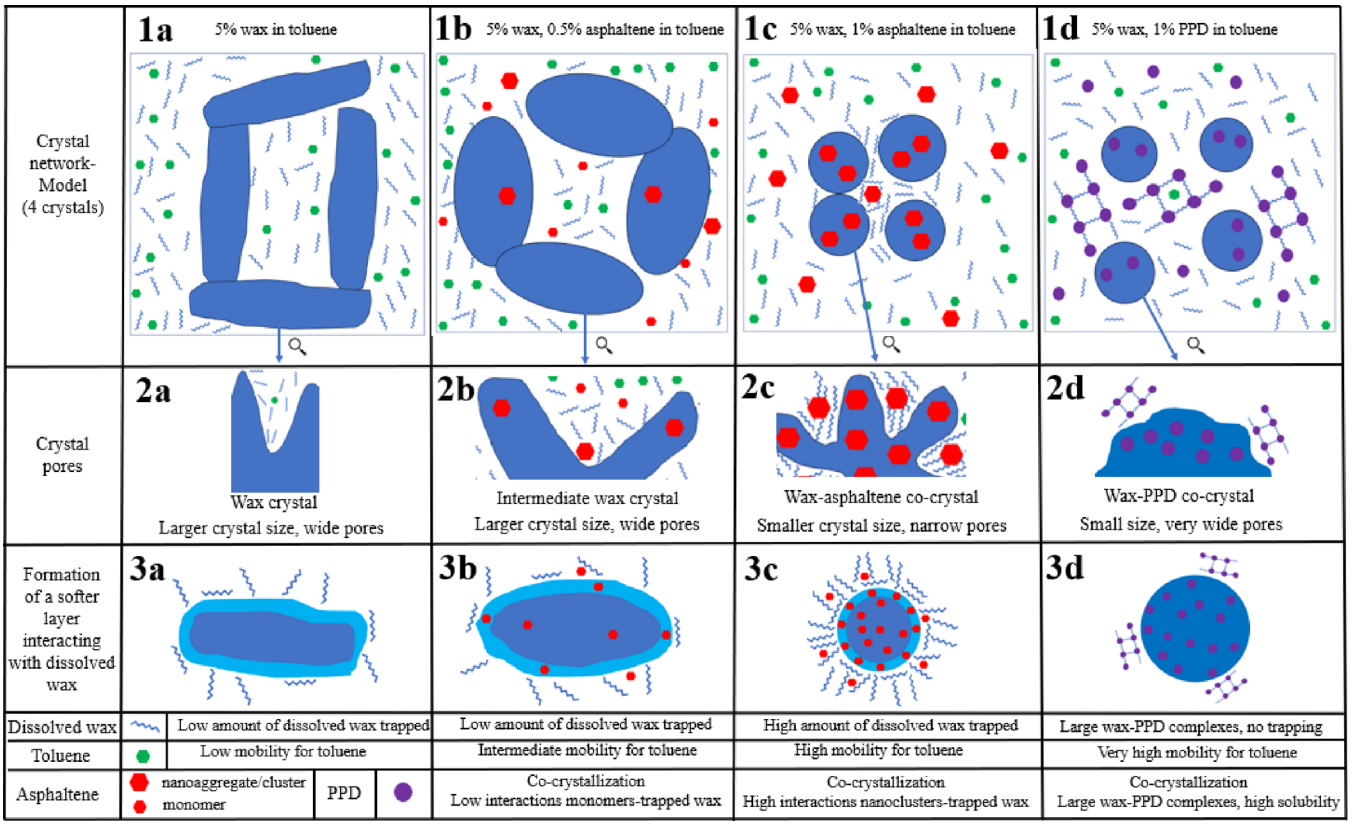

Supporting Information, respectively. As expected, the presence of asphaltenes generated a much more significant decrease at 0 °C than at 10 °C. The presence of PPD had a comparable effect at 0 °C. This demonstrated that the solvent pathway through the crystal network became less convoluted when wax crystals were altered by asphaltenes or PPDs.

The tortuosity analysis can be correlated with results in the previous study by Savulescu et al.[19] The formation of a low-mobility dissolved wax region at a low temperature was identified in wax and wax−asphaltene systems. Different trends were observed for dissolved wax and toluene when asphaltenes were present. Although the previous study found that higher asphaltene concentrations increased the amount of trapped dissolved wax, the tortuosity measurements decreased the restriction on toluene molecules when the asphaltene content increased. The explanation for this lies in the nature of the chemical structures of wax and toluene. The dissolved wax at low mobility can interact with asphaltene nanoaggregates, which behave either as wax crystal network binders or as nucleation sites. On the other hand, toluene does not interact with the other components during this process.

Asphaltenes and PPDs have a different mechanism of interaction with wax during precipitation. PPDs reduce wax solubility through the formation of liquid complexes, which then precipitate as a modified wax−PPD crystal network.[5] On the other hand, asphaltenes are highly unlikely to alter wax crystals until the gelation phase. This can also be observed in the results in Figures 8 and 9. The PPD had an inhibiting effect on the wax precipitation at 10 °C, delaying the formation of a strong solid network. On the other hand, wax precipitation was in more advanced stages (higher viscosity) in the wax−asphaltene systems at 10 °C. At 0 °C, when gelation and precipitation were rapidly occurring, the restricted diffusion was 6−9 times higher when asphaltenes were present and asphaltene concentration had a distinguishable effect.

Another thing to mention is that the restricted diffusion coefficient for wax−PPD at 0 °C was higher than the restricted diffusion coefficient of wax at 10 °C. This illustrated a delay of over 10 °C in restriction on the solvent movement through the wax crystal network when 1% PPD was added. The same could be observed for the system with the highest asphaltene concentration (2%). One can conclude that although asphaltenes at high concentration were found to promote wax precipitation (i.e., higher crystallized amount)[19] and to intensify the amount of low-mobility dissolved wax, the resulting crystals had modified properties that increased the restricted solvent diffusion. In real systems, this would translate to a higher quantity of wax but with more open networks, giving a better flowability for the liquid components in the crude oil.

3.4. Interpretation of the Wax Crystal and Network Structures. Our interpretation of the influence of asphaltenes and PPDs on the wax crystal and network structures in toluene is summarized in this section. Scheme 1 shows an overview of cross sections of the different wax systems below the WAT that have been studied. The first line (1a−1d) illustrates crystal networks, represented by four crystals for simplicity. The second line (2a−2d) illustrates part of single crystals with varying porosity, while single crystals are drawn on the third line (3a−3d).

The wax network formed with only wax dissolved in toluene was considered as the reference case. It is well known that elongated wax crystals form in such systems[26] and that these crystals interlock to form a porous network. This was

https://doi.org/10.1021/acs.iecr.3c02218
Ind. Eng. Chem. Res. XXXX, XXX, XXX−XXX

confirmed by the strongly reduced mobility of solvent molecules (toluene) in Figure 8 and 9. Previously, a population of wax with intermediate mobility, i.e., mobility between that of liquid and solid wax, was identified below the WAT.[44] Several possibilities for the origin of this population have been put forward: trapping of wax molecules between the interlocking wax crystals[19,44] (illustrated in Scheme 1, 1a), formation of pores within the precipitated wax crystal containing less mobile wax[12,26] (illustrated in Scheme 1, 2a), and an amorphous, softer layer of less mobile wax surrounding the wax crystals[44] (illustrated in Scheme 1, 3a). All these mechanisms need further verification but are nevertheless considered in the following discussion of how the presence of asphaltenes and PPD can alter the wax crystal network.

The presence of asphaltenes was considered first. The amount of asphaltenes significantly influenced the wax precipitation and network structures significantly. Below a threshold range (about 0.75−1% asphaltenes in 5% wax), asphaltene monomers were predominantly present. In this concentration range, asphaltenes induced rounder wax−asphaltene cocrystals, with less interlocking and wider, less deep pores (Scheme 1 and Figures 1b−3b). This was shown by the increase in toluene mobility and ongoing atomic force microscopy studies. The low amount of nanoaggregates in this concentration range did not have a significant impact on wax crystallization in the nucleation stage. The low content of asphaltenes, relative to wax (<1:7), also induced a lower likelihood for asphaltene monomers and nanoaggregates to act as wax crystal binders. This resulted in a crystal network that resembled wax-only systems in the way that it had similar capacity to trap wax.[19]

Above the threshold range (>1% asphaltene), mostly asphaltene nanoaggregates and nanoclusters were present. These acted as nucleation sites for wax due to the formation of a larger nonpolar region after nanoaggregation/nanoclustering and/or due to the increased surface area for heterogeneous nucleation.[9] During the initial stages of nucleation and growth, the nonpolar parts of asphaltene aggregates might interact with the nonpolar wax molecules through London forces[10,11] and lead to cocrystallization of wax and asphaltene aggregates. The incorporation of asphaltene nanoclusters in the wax crystals also imposed steric hindrances that restricted their growth,[12] resulting in smaller cocrystals with rounder shapes.[26] These cocrystals might be packed closer and formed network structures with smaller confinements between individual crystals (Figures 8 and 9). Moreover, higher amounts of liquid wax with reduced mobility were found in these structures.[19] This wax population occurs due to the same mechanisms as outlined above: trapping of wax in a more confined space between the smaller interlocked cocrystals (Scheme 1, 1c), less mobile wax in smaller pores of the wax−asphaltene aggregate cocrystals (Scheme 1, 2c), and the presence of a softer, amorphous wax−asphaltene layer surrounding the cocrystals that possibly also interacted with dissolved wax (Scheme 1, 3c).

Notably, the population of dissolved wax with reduced mobility increases, while dissolved toluene had an increase in mobility in these structures in comparison to the wax-only system. This demonstrated that the trapping of dissolved wax was not only caused by spatial hindrance due to gaps in the crystal networks and pores but could have reduced the mobility of toluene as well. An additional factor was most likely interactions of dissolved wax with the species in the altered wax−asphaltene crystal network or with species undergoing nucleation/gelation[19] (Scheme 1, 2c−3c).

Finally, the presence of polycarboxylate PPD also had a marked effect on the crystal network formed upon crystallization. Also in this case, interactions between hydrophobic segments of the PPD and wax during the nucleation and growth stage were considered to give rise to cocrystallization of wax and PPD. Steric hindrance provided by the PPD on growing crystals limited the cocrystal growth, giving smaller and rounder crystals similar to those formed in the presence of asphaltene aggregates. The geometry of the resulting cocrystal networks, however, was markedly different in the way that the wax−PPD networks had less interconnections between the cocrystals and hence were more open (Figures 8 and 9). Also, the wax−PPD complexes in the liquid state were significantly larger, requiring more space to crystallize, which delayed crystallization and improved solubility (Scheme 1, 1d): PPD at 1% reduced the wax crystallization rate significantly.[19] The wax−PPD cocrystal network did not trap dissolved wax molecules.[19] The crystal network formation did not follow any of the 3 mechanisms proposed for wax and wax−asphaltene systems for dissolved wax trapping. First, there is little interlocking and wide gaps between individual crystals (Scheme 1, 1d). Second, ongoing atomic force microscopy studies show no noticeable pore structure (Scheme 1, 2d). Last, intermediate amorphous phases were not recorded with any of the proposed experimental techniques or ongoing studies (Scheme 1, 3d).

4. CONCLUSIONS

This study highlighted novel approaches that consolidated the knowledge about wax−modifier interactions using improved NMR techniques to overcome the limitations of previous wax crystallization characterization methods:

1 Identification and quantification of asphaltene-specific and PPD-specific peaks at various temperatures were performed with high-resolution NMR, leading to the demonstration of wax−asphaltene and wax−PPD cocrystallization. This confirmed cocrystallization as a factor for changes in wax crystal behavior. Moreover, the approach could be used in future research to compare the behavior of systems with different degrees of cocrystallization.

2 Changes in molecular mobility with increasing asphaltene concentration were detected with NMR CPMG in asphaltene-only systems. A shift toward low mobility peaks was noticed above a threshold concentration. The same concentration corresponded to the asphaltene concentration at which the wax−asphaltene crystals provided spatial hindrance on dissolved wax molecules, trapping them and preventing further crystal growth. This demonstrated the nanoaggregation of asphaltenes and its impact on the modification of wax crystallization behavior. The determination of the monomer:nanoaggregate ratio inside the liquid-specific mobility region consolidated previous SANS and SAXS studies that proved the existence of these nanoaggregates.

3 The effect of crystal modification on the tortuosity and free diffusion of the solvent was assessed using pulsed field gradient NMR. Higher diffusion of solvent molecules through the wax crystal network was recorded when asphaltenes were present, and even higher values

https://doi.org/10.1021/acs.iecr.3c02218
Ind. Eng. Chem. Res. XXXX, XXX, XXX−XXX

were obtained with PPD. This represented a quantitative measure of the effects of wax crystal alteration, weaker, smaller, and more finely dispersed crystals, which allowed for higher flowability.

■ ASSOCIATED CONTENT

Supporting Information

The Supporting Information is available free of charge at https://pubs.acs.org/doi/10.1021/acs.iecr.3c02218.

Additional figures that clarify observations in the main paper (PDF)

■ AUTHOR INFORMATION

Corresponding Author

George Claudiu Savulescu − *Ugelstad Laboratory, Norwegian University of Science and Technology, Trondheim 7491, Norway;* orcid.org/0000-0003-3278-0745; Email: george.c.savulescu@ntnu.no

Authors

Sébastien Simon − *Ugelstad Laboratory, Norwegian University of Science and Technology, Trondheim 7491, Norway*

Geir Sørland − *Ugelstad Laboratory, Norwegian University of Science and Technology, Trondheim 7491, Norway; Anvendt Teknologi AS, Trondheim 7022, Norway*

Gisle Øye − *Ugelstad Laboratory, Norwegian University of Science and Technology, Trondheim 7491, Norway;* orcid.org/0000-0002-6391-3750

Complete contact information is available at: https://pubs.acs.org/10.1021/acs.iecr.3c02218

Notes

The authors declare no competing financial interest.

■ ACKNOWLEDGMENTS

This work is part of SUBPRO SFI, a research-based center within subsea production and processing. The authors hereby acknowledge the financial support from SUBPRO, which is financed by the Research Council of Norway, major industry partners and NTNU.

■ REFERENCES

(1) Oliveira, L. M. S. L.; Nunes, R. C. P.; Melo, I. C.; Ribeiro, Y. L. L.; Reis, L. G.; Dias, J. C. M.; Guimarães, R. C. L.; Lucas, E. F. Evaluation of the Correlation between Wax Type and Structure/Behavior of the Pour Point Depressant. *Fuel Process. Technol.* **2016**, *149*, 268−274.

(2) Yang, F.; Zhao, Y.; Sjöblom, J.; Li, C.; Paso, K. G. Polymeric Wax Inhibitors and Pour Point Depressants for Waxy Crude Oils: A Critical Review. *J. Dispersion Sci. Technol.* **2015**, *36*, 213−225.

(3) Kelland, M. A. *Production Chemicals for the Oil and Gas Industry*; 2009; Vol. *1*. CRC Press.

(4) Al-Yaari, M. Paraffin Wax Deposition: Mitigation and Removal Techniques. *SPE - Saudi Arabia Section Young Professionals Technical Symposium (conference)*. paper nr. SPE-155412-MS. 2011.

(5) Paso, K. G.; Krückert, K. K.; Oschmann, H.-J.; Ali, H.; Sjöblom, J. PPD Architecture Development via Polymer−Crystal Interaction Assessment. *J. Pet. Sci. Eng.* **2014**, *115*, 38−49.

(6) Wei, B. Recent Advances on Mitigating Wax Problem Using Polymeric Wax Crystal Modifier. *J. Pet. Explor. Prod. Technol.* **2015**, *5* (4), 391−401.

(7) Bai, Y.; Bai, Q. 16 - Wax and Asphaltenes. In *Subseas Engineering Handbook*; Second edition Eds.; Gulf Professional Publishing: Boston, 2019; pp 435−453.

(8) Mullins, O. C.; Sabbah, H.; Eyssautier, J.; Pomerantz, A. E.; Barré, L.; Andrews, A. B.; Ruiz-Morales, Y.; Mostowfi, F.; McFarlane, R.; Goual, L.; Lepkowicz, R.; Cooper, T.; Orbulescu, J.; Leblanc, R. M.; Edwards, J.; Zare, R. N. Advances in asphaltene Science and the Yen−Mullins Model. *Energy Fuels* **2012**, *26* (7), 3986−4003.

(9) Kriz, P.; Andersen, S. I. Effect of Asphaltenes on Crude Oil Wax Crystallization. *Energy Fuels* **2005**, *19* (3), 948−953.

(10) Lei, Y.; Han, S.; Zhang, J.; Bao, Y.; Yao, Z.; Xu, Y. Study on the Effect of Dispersed and Aggregated asphaltene on Wax Crystallization, Gelation, and Flow Behavior of Crude Oil. *Energy Fuels* **2014**, *28* (4), 2314−2321.

(11) Ariza-León, E.; Molina-Velasco, D.-R.; Chaves-Guerrero, A. REVIEW OF STUDIES ON asphaltene - WAX INTERACTION AND THE EFFECT THEREOF ON CRYSTALLIZATION. *CT&F - Cienc., Tecnol. Futuro* **2014**, *5*, 39−53.

(12) Cao, H.; Cao, X.; Zhao, X.; Guo, D.; Liu, Y.; Bian, J. Molecular Dynamics Simulation of Wax Molecules Aggregational Crystallization Behavior during Cooling of Crude Oil Mixture. *Case Stud. Therm. Eng.* **2022**, *37*, No. 102298.

(13) Venkatesan, R.; Östlund, J.-A.; Chawla, H.; Wattana, P.; Nydén, M.; Fogler, H. S. The Effect of Asphaltenes on the Gelation of Waxy Oils. *Energy Fuels* **2003**, *17* (6), 1630−1640.

(14) Oliveira, G. E.; Mansur, C. R. E.; Lucas, E. F.; González, G.; de Souza, W. F. The Effect of Asphaltenes, Naphthenic Acids, and Polymeric Inhibitors on the Pour Point of Paraffins Solutions. *J. Dispersion Sci. Technol.* **2007**, *28* (3), 349−356.

(15) García, M. D. C. Crude Oil Wax Crystallization. The Effect of Heavy n-Paraffins and Flocculated Asphaltenes. *Energy Fuels* **2000**, *14* (5), 1043−1048.

(16) Molina, V. D.; Ariza León, E.; Chaves-Guerrero, A. Understanding the Effect of Chemical Structure of Asphaltenes on Wax Crystallization of Crude Oils from Colorado Oil Field. *Energy Fuels* **2017**, *31* (9), 8997−9005.

(17) García, M. D. C.; Carbognani, L. asphaltene−Paraffin Structural Interactions. Effect on Crude Oil Stability. *Energy Fuels* **2001**, *15* (5), 1021−1027.

(18) Lei, Y.; Han, S.; Zhang, J. Effect of the Dispersion Degree of asphaltene on Wax Deposition in Crude Oil under Static Conditions. *Fuel Process. Technol.* **2016**, *146*, 20−28.

(19) Savulescu, G. C.; Simon, S.; Sørland, G.; Øye, G. New Nuclear Magnetic Resonance Approaches on the Evolution of Wax Mobility during Wax Crystallization. *Energy Fuels* **2022**, *36* (1), 350−360.

(20) Savulescu, G. C.; Simon, S.; Sørland, G.; Øye, G. Novel Nuclear Magnetic Resonance Techniques To Assess the Wax Precipitation Evolution in Crude Oil Systems. *Energy Fuels* **2023**, *37* (1), 291−300.

(21) Kurniawan, M.; Subramanian, S.; Norrman, J.; Paso, K. Influence of Microcrystalline Wax on the Properties of Model Wax-Oil Gels. *Energy Fuels* **2018**, *32* (5), 5857−5867.

(22) Pedersen, W. B.; Baltzer Hansen, A.; Larsen, E.; Nielsen, A. B.; Roenningsen, H. P. Wax Precipitation from North Sea Crude Oils. 2. Solid-Phase Content as Function of Temperature Determined by Pulsed NMR. *Energy Fuels* **1991**, *5* (6), 908−913.

(23) Slichter, C. P. *Principles of Magnetic Resonance*; Springer Science & Business Media: Springer-Verlag Berlin Heidelberg, 2013.

(24) Meiboom, S.; Gill, D. Modified Spin-Echo Method for Measuring Nuclear Relaxation Times. *Rev. Sci. Instrum.* **1958**, *29* (8), 688−691.

(25) Zhao, Y.; Paso, K.; Norrman, J.; Ali, H.; Sørland, G.; Sjöblom, J. Utilization of DSC, NIR, and NMR for Wax Appearance Temperature and Chemical Additive Performance Characterization. *J. Therm. Anal. Calorim.* **2015**, *120* (2), 1427−1433.

(26) Ruwoldt, J.; Humborstad Sørland, G.; Simon, S.; Oschmann, H.-J.; Sjöblom, J. Inhibitor-Wax Interactions and PPD Effect on Wax Crystallization: New Approaches for GC/MS and NMR, and

Comparison with DSC, CPM, and Rheometry. *J. Pet. Sci. Eng.* **2019**, *177*, 53−68.
(27) Subramanian, S.; Sørland, G. H.; Simon, S.; Xu, Z.; Sjöblom, J. asphaltene Fractionation Based on Adsorption onto Calcium Carbonate: Part 2. Self-Association and Aggregation Properties. *Colloids Surf., A* **2017**, *514*, 79−90.
(28) Pinto, F. E.; Barros, E. V.; Tose, L. V.; Souza, L. M.; Terra, L. A.; Poppi, R. J.; Vaz, B. G.; Vasconcelos, G.; Subramanian, S.; Simon, S.; Sjöblom, J.; Romão, W. Fractionation of Asphaltenes in N-Hexane and on Adsorption onto CaCO3 and Characterization by ESI(+)FT-ICR MS: Part I. *Fuel* **2017**, *210*, 790−802.
(29) Sørland, G. H.; Anthonsen, H. W.; Ukkelberg, Å.; Zick, K. A Robust Method for Analysing One and Two-Dimensional Dynamic NMR Data. *Appl. Magn. Reson.* **2022**, *53* (10), 1345−1359.
(30) Andrews, A. B.; Guerra, R. E.; Mullins, O. C.; Sen, P. N. Diffusivity of asphaltene Molecules by Fluorescence Correlation Spectroscopy. *J. Phys. Chem. A* **2006**, *110* (26), 8093−8097.
(31) Chen, W.; Zhao, H.; Xue, Y.; Chang, X. Adsorption Effect and Adsorption Mechanism of High Content Zeolite Ceramsite on Asphalt VOCs. *Materials* **2022**, *15*, 6100.
(32) Sørland, G. H.; Hafskjold, B.; Herstad, O. A Stimulated-Echo Method for Diffusion Measurements in Heterogeneous Media Using Pulsed Field Gradients. *J. Magn. Reson.* **1997**, *124* (1), 172−176.
(33) Sørland, G. H.; Aksnes, D.; Gjerdåker, L. A Pulsed Field Gradient Spin-Echo Method for Diffusion Measurements in the Presence of Internal Gradients. *J. Magn. Reson.* **1999**, *137* (2), 397−401.
(34) Mitra, P. P.; Sen, P. N.; Schwartz, L. M.; Le Doussal, P. Diffusion Propagator as a Probe of the Structure of Porous Media. *Phys. Rev. Lett.* **1992**, *68* (24), 3555−3558.
(35) Tourell, M. C.; Pop, I.-A.; Brown, L. J.; Brown, R. C. D.; Pileio, G. Singlet-Assisted Diffusion-NMR (SAD-NMR): Redefining the Limits When Measuring tortuosity in Porous Media. *Phys. Chem. Chem. Phys.* **2018**, *20* (20), 13705−13713.
(36) Latour, L. L.; Mitra, P. P.; Kleinberg, R. L.; Sotak, C. H. Time-Dependent Diffusion Coefficient of Fluids in Porous Media as a Probe of Surface-to-Volume Ratio. *J. Magn. Reson. Ser. A* **1993**, *101* (3), 342−346.
(37) Wu, C.; Zhang, J.; Li, W.; Wu, N. Molecular Dynamics Simulation Guiding the Improvement of EVA-Type Pour Point Depressant. *Fuel* **2005**, *84* (16), 2039−2047.
(38) Espinat, D.; Fenistein, D.; Barré, L.; Frot, D.; Briolant, Y. Effects of Temperature and Pressure on Asphaltenes Agglomeration in Toluene. A Light, X-Ray, and Neutron Scattering Investigation. *Energy Fuels* **2004**, *18* (5), 1243−1249.
(39) Roux, J.-N.; Broseta, D.; Demé, B. SANS Study of asphaltene Aggregation: Concentration and Solvent Quality Effects. *Langmuir* **2001**, *17* (16), 5085−5092.
(40) Eyssautier, J.; Levitz, P.; Espinat, D.; Jestin, J.; Gummel, J.; Grillo, I.; Barré, L. Insight into asphaltene Nanoaggregate Structure Inferred by Small Angle Neutron and X-Ray Scattering. *J. Phys. Chem. B* **2011**, *115* (21), 6827−6837.
(41) Eyssautier, J.; Hénaut, I.; Levitz, P.; Espinat, D.; Barré, L. Organization of Asphaltenes in a Vacuum Residue: A Small-Angle X-Ray Scattering (SAXS)−Viscosity Approach at High Temperatures. *Energy Fuels* **2012**, *26* (5), 2696−2704.
(42) Barré, L.; Jestin, J.; Morisset, A.; Palermo, T.; Simon, S. Relation between Nanoscale Structure of asphaltene Aggregates and Their Macroscopic Solution Properties. *Oil Gas Sci. Technol. - Rev. IFP* **2009**, *64* (5), 617−628.
(43) van de Ree, J. Classical Trajectory Calculations of the Scattering of TlF on Ar in Thermal Beams. *J. Chem. Phys.* **1971**, *54* (8), 3249−3262.
(44) Morozov, E. V.; Nizovtseva, P. V.; Martyanov, O. N. From Components to Phase-Dependent Dynamics of Diffusivity in Wax Solutions Subjected to Fluid−Solid Phase Transition: Insights from Pulsed Field Gradient NMR. *Energy Fuels* **2022**, *36* (24), 14696−14709.

https://doi.org/10.1021/acs.iecr.3c02218
Ind. Eng. Chem. Res. XXXX, XXX, XXX−XXX